

Understanding radiative transfer in the midwave infrared, a precursor to full spectrum atmospheric compensation

Michael K. Griffin^{*}, Hsiao-hua K. Burke, John P. Kerekes
MIT Lincoln Laboratory, 244 Wood Street, Lexington, MA, USA 02420-9185

ABSTRACT

The compensation for atmospheric effects in the VNIR/SWIR has reached a mature stage of development with many algorithms available for application (ATREM, FLAASH, ACORN, etc.). Compensation of LWIR data is the focus of a number of promising algorithms. A gap in development exists in the MWIR where little or no atmospheric compensation work has been done yet an increased interest in MWIR applications is emerging. To obtain atmospheric compensation over the full spectrum (visible through LWIR), a better understanding of the radiative effects in the MWIR is needed. The MWIR is characterized by a unique combination of reduced solar irradiance and low thermal emission (for typical emitting surfaces), both providing relatively equal contributions to the daytime MWIR radiance. In the MWIR and LWIR, the compensation problem can be viewed as two interdependent processes: compensation for the effects of the atmosphere and the uncoupling of the surface temperature and emissivity. The former requires calculations of the atmospheric transmittance due to gases, aerosols, and thin clouds and the path radiance directed towards the sensor (both solar scattered and thermal emissions in the MWIR). A framework for a combined MWIR/LWIR compensation approach is presented where both scattering and absorption by atmospheric particles and gases are considered.

Keywords: MWIR, LWIR, hyperspectral, atmospheric compensation, radiative transfer

1. INTRODUCTION

Hyperspectral imaging sensors have been used to aid in the detection and identification of diverse surface elements, topographical, and geological features, ambient dust and aerosols, smoke from fires, as well as suspended gaseous effluents. Hyperspectral data are not immune to the effects of the intervening atmosphere. The term “atmospheric compensation” refers to the removal of unwanted atmospheric components of the measured radiance so that an estimate of the surface leaving radiance or reflectance can be obtained. For hyperspectral data analysis in the reflected solar spectral regime, the general objective of atmospheric compensation algorithms is to remove solar illumination and atmospheric effects (predominantly aerosol scattering and water vapor absorption) from the measured spectral data so that an accurate estimate of the surface reflectance can be obtained¹. In the thermal emissive region of the spectrum, the objective is two-fold: 1) remove atmospheric components of the sensor-measured radiance to obtain a ground-leaving radiance, and 2) separate the temperature and emissivity components from the retrieved radiance, the primary product being an estimate of the surface spectral emissivity.

Difficulties can arise when atmospheric conditions are stressing (e.g., high moisture, heavy aerosol/particulate loading, partial cloud cover, low sun angle). The effects are further enhanced when the measured signal is low (over low reflectance or cold surfaces or for spectral regions of low solar or thermal radiance). In the MWIR (3 – 6 μm), the reflected solar radiance is quite small compared to that in the VNIR and the thermal emissive radiance for normal surface and atmospheric conditions is also at a minimum. These factors provide a unique challenge to those who attempt to derive information from MWIR data. The following sections will highlight the typical spectral and radiometric signatures to be found in the MWIR for different scenarios. The equations governing the transfer of radiation in this regime will also be examined.

^{*}griffin@ll.mit.edu; Voice: 781-981-0396; FAX: 781-981-7271

2. MWIR SPECTRAL CHARACTERISTICS

To estimate the underlying surface-leaving radiance from a remote airborne or spaceborne platform, the effects of the intervening atmosphere must be considered. Typically, at MWIR wavelengths, the radiative flux is impacted by the absorption by well-mixed gases such as Ozone (O_3), Oxygen (O_2), Nitrogen (N_2), Methane (CH_4), Nitrous Oxide (N_2O), Nitrogen Dioxide (NO_2) and Carbon Dioxide (CO_2), and the absorption by water vapor. Mixed gases can be modeled accurately and play an important role in the retrieval of specific properties of the earth-atmosphere system².

Figure 1 provides examples of the atmospheric absorption (defined as $1 - \text{transmittance}$) over the spectral region from 2.5 to 7 μm for two atmospheric conditions: 1) clear and dry and 2) hazy and humid. The curves were produced with Modtran³ over a full (100 km) nadir atmospheric path. These cases produce values for atmospheric absorption that represent the extreme bounds for a nominal atmosphere. It is clear that the MWIR spectral band is dominated by strongly absorbing gases. One moderately transmissive “window” region exists between 3 and 4 microns with minimum absorption near 3.8 μm for dry atmospheres and 3.9 μm for moist atmospheres. A second transmissive region exists between 4.6 and 5.4 μm with minimum absorption values near 4.6 μm . In contrast with the VNIR/SWIR spectral band, which exhibits numerous atmospheric windows, the MWIR has limited spectral regions for retrieving surface information.

The absorption curves in Fig. 1 can be divided into contributions from individual gases and aerosols. From Fig. 2 it can be seen that numerous gases have absorption features in the MWIR; the absorption curves for ten gases including water vapor are plotted. Water vapor is the major absorber in the MWIR and provides the bulk of the total atmospheric absorption shown in Fig. 1. Since the amount of water vapor in the atmosphere varies greatly both spatially and temporally, its effect on transmission in the MWIR can also vary. Plotted in Fig. 2 is the water vapor absorption for the dry case shown in Fig. 1, which represents an estimate of the minimum absorption to be expected. Two major H_2O absorption bands are found in the MWIR: a strong band near 2.7 μm and the major water vapor complex of lines near 6.7 μm . The latter band spans over 3 μm from 5 to 8 μm and represents a primary region of the spectrum for obtaining information used to retrieve layered atmospheric water vapor amounts. It can be seen that the water vapor absorption overwhelms weaker absorption by other gases, even for relatively dry atmospheres.

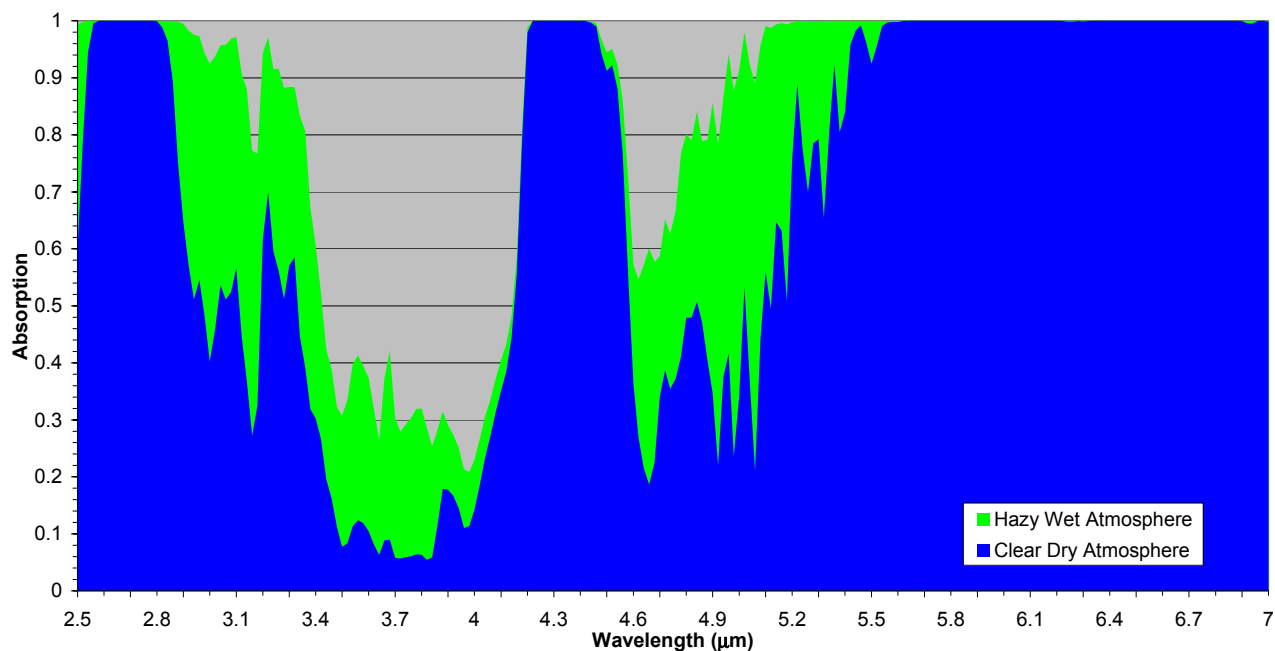


Figure 1. Plots of the atmospheric absorption across the MWIR spectral region for two atmospheric conditions: hazy/wet and clear/dry.

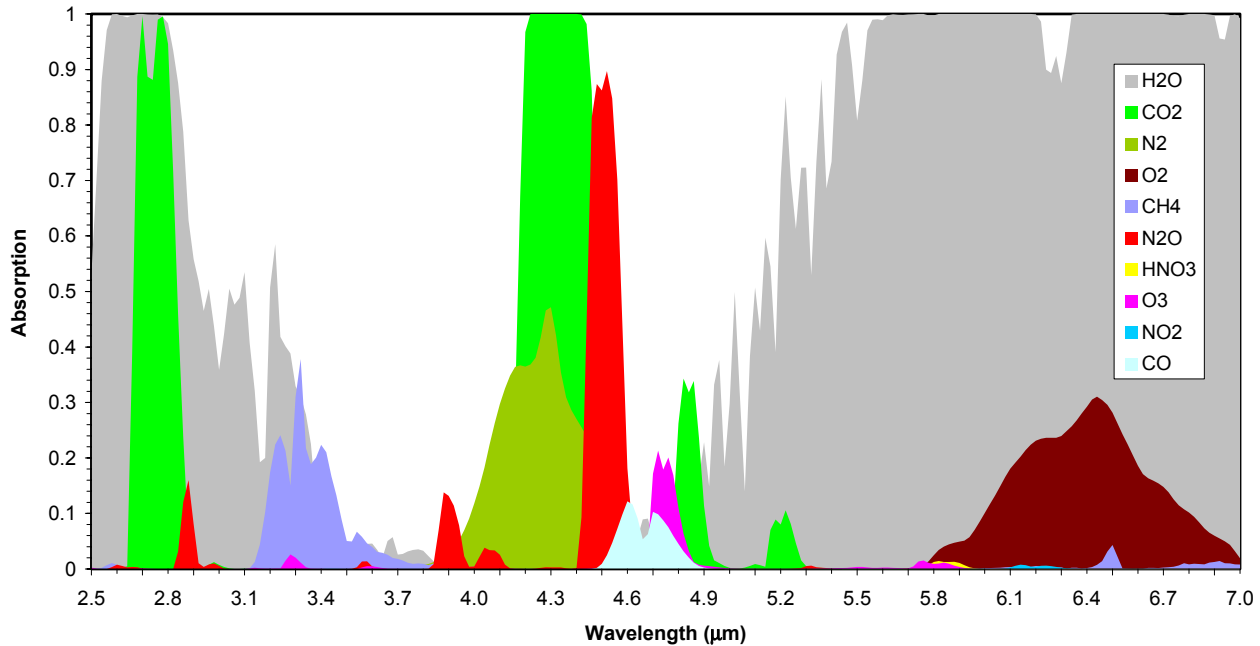


Figure 2. Plots of the nominal ambient atmospheric absorption for 10 molecular species that exhibit absorption features in the MWIR.

Carbon dioxide absorbs strongly between 4.1 and 4.4 μm and also near 2.8 μm . The 2.7 μm H₂O absorption mostly eclipses the latter CO₂ band. CO₂ also exhibits a moderate absorption line at 4.85 and 5.2 μm ; the effects of both are diminished by water vapor. Absorption by CO₂ at 4.25 μm is strong enough to provide the opportunity to estimate atmospheric temperatures in the Stratosphere using retrieval algorithms. Adjacent to this CO₂ band is a strong N₂O absorption band centered at 4.5 μm . Weaker bands are also found at 2.9, 3.9 and 4.05 μm , but only the 3.9 μm band falls within the MWIR window. Molecular nitrogen also displays a broad area of moderate absorption at 4.3 μm , the effect being to broaden the CO₂ absorption region to 3.9 μm . A moderate CH₄ absorption band is located near 3.3 μm on the edge of the water vapor band and extending into the MWIR window. Minor O₃ absorption is present at 4.75 μm ; CO displays minor absorption from 4.5 to 4.9 μm . Other gases, such as O₂, NO₂ and HNO₃ as well as CH₄ and O₃ display absorption from 5.5 to 7 μm , but the effects are completely encompassed by the expansive water vapor band.

Scattering by molecules is negligible at these wavelengths⁴, and scattering and absorption by normal atmospheric aerosols produces transmission losses between 2 and 15 percent depending on the aerosol type and visibility. In contrast to the MWIR, transmission losses due to aerosols in the VNIR/SWIR are typically two to three times that amount. Typical absorption loss based on Modtran³ aerosol modeling is limited to 1 – 4 percent with minimum absorption occurring for maritime aerosols and maximum absorption found in urban aerosols that tend to contain significant amounts of carbon. Figure 3 displays plots of the scattering and absorption across the MWIR for the two extreme aerosol conditions used in the calculations for the Fig. 1 curves. The scattering from aerosols is found to vary slowly and continuously with wavelength with a slight decrease in transmission loss towards longer wavelengths in the MWIR. Models have been developed based upon the size and near-spherical shape of aerosols to estimate the effects of scattering on the transmission of solar and thermal energy in the atmosphere⁵.

2.1 Surface Emissivity

Two parameters define the effects of the surface in (4), the surface temperature and emissivity. In (4), T_s represents the surface skin or radiative temperature, which can differ dramatically from the more commonly used surface air

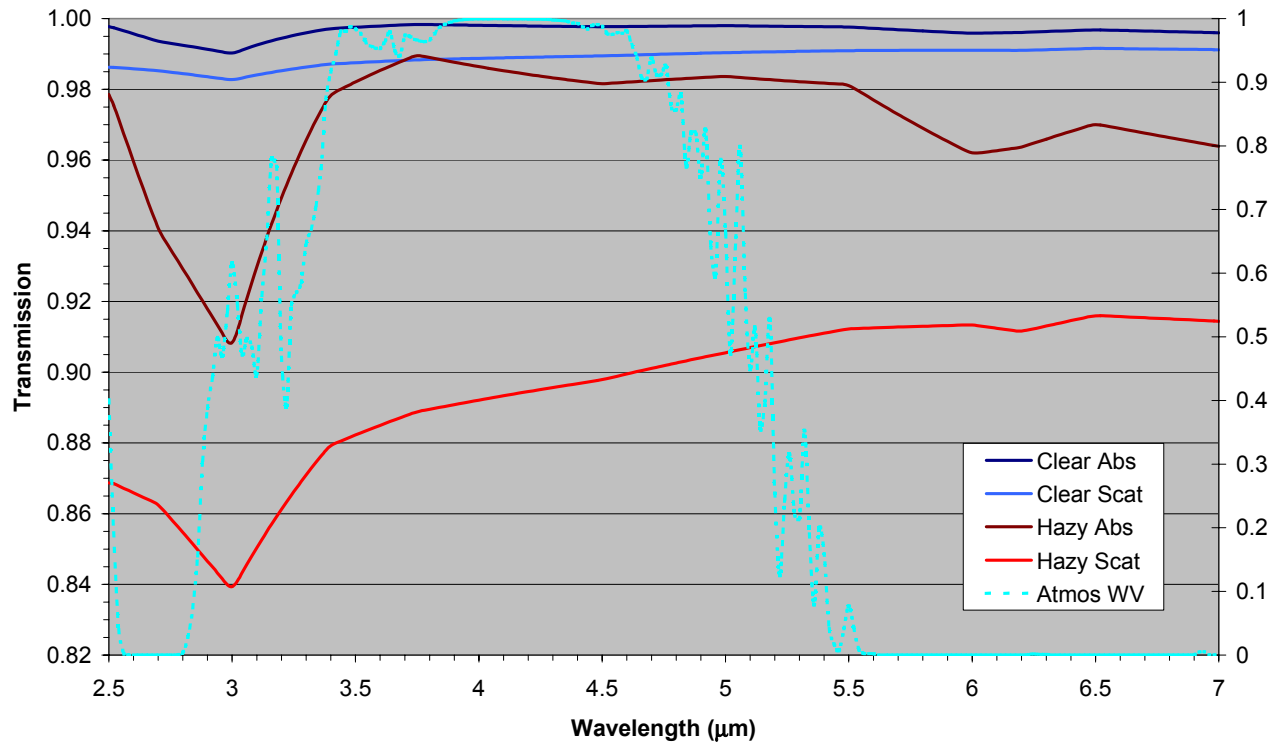


Figure 3. Aerosol transmission curves due to absorption and scattering are plotted for the MWIR spectral region for two different conditions. Atmospheric water vapor transmission is also shown for comparison (right axis corresponds to the water vapor values).

temperature. The surface emissivity ϵ_s which is assumed here to be $1 - \rho_s$, the surface reflectance, is generally characterized by values above 0.85 in the MWIR and LWIR⁶. Figure 4 provides examples of the surface emissivity for four surface types: asphalt, concrete, conifer trees, and grass. Values in the MWIR window range from 0.92-0.94 for manmade surfaces such as concrete and asphalt to 0.99 for natural surface features such as grass and trees. The values suggest that only a small percentage of the downwelling solar or thermal signal will be reflected and retransmitted up to the sensor.

3. MWIR RADIOMETRIC CHARACTERISTICS

In the VNIR, scattering of the sun's energy by the earth-atmosphere system dominates the radiative transfer; thermally emitted radiance is negligible for almost all conditions (fires can be an exception⁷). The opposite is true for the LWIR, where the thermal emission from the earth and atmosphere dominate. The MWIR spectral region is unique in that it is not situated near the peak of a source of emission in the temperature regime of interest and the solar contribution is greatly reduced. Solar radiation has no component in the transfer of radiation in the LWIR, however, the absorption of solar radiation by the earth and the atmosphere will alter the temperature and the resultant re-emission in the LWIR. Between the two spectral regions where contributions from both sources are important, the radiative transfer is more complex with both scattering and absorption effects needing consideration. In Figure 5, examples of the total radiance for the two cases used in Fig. 1 are given. TOA radiances were computed using Modtran with a constant (0.05) surface reflectance. A radiance minimum is seen near 2.7 μm where water vapor absorption and low solar radiance combine to minimize the reflected radiance. The difference in the two curves is small through the MWIR window region, beyond which water vapor absorption produces an increasing separation in the total radiance curves. The absolute radiance is typically below $1 \text{ W/m}^2\text{-sr-}\mu\text{m}$ through the MWIR window with increasingly higher values ($1 - 4 \text{ W/m}^2\text{-sr-}\mu\text{m}$) beyond the CO_2 absorption band.

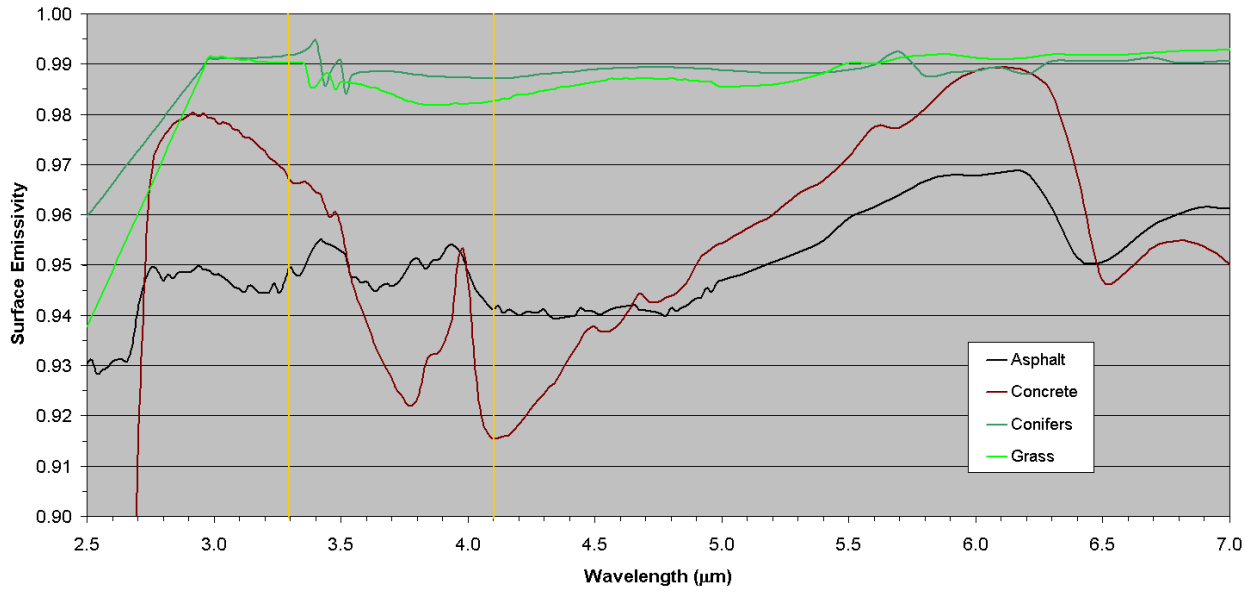


Figure 4. Graphs of the surface emissivity in the MWIR for four surface materials are shown. The vertical lines denote the nominal bounds for the MWIR atmospheric window region.

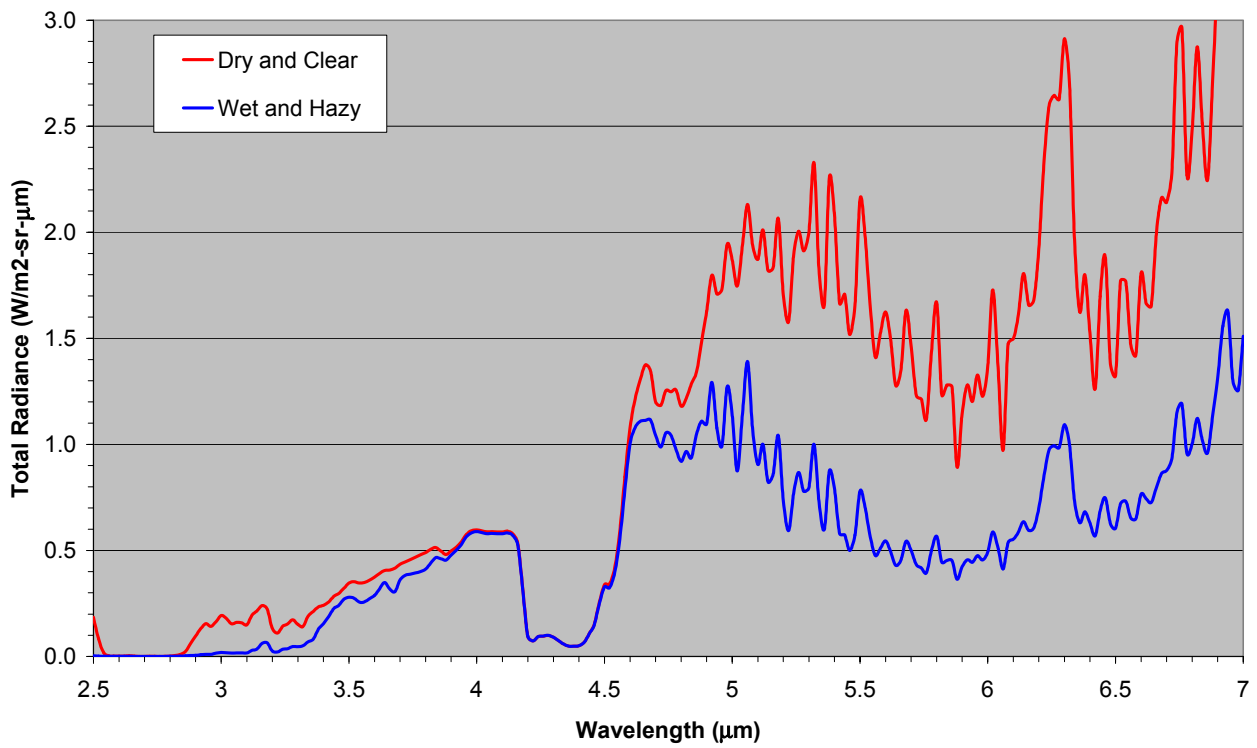


Figure 5. Curves depicting the MWIR radiance that reaches the TOA from a surface of constant (0.05) reflectance and two sets of atmospheric conditions, 1) dry and clear, and 2) wet and hazy.

Figure 6 provides a plot of the individual components of the radiative transfer: surface emitted thermal radiance, surface reflected downwelling solar and thermal radiance, thermal path radiance, and reflected path solar radiance. The magnitude of each component is shown as a fraction of the total radiance received at the TOA. The left plot represents values for dry and clear atmospheric conditions and the plot on the right for a wet and hazy scene. The magnitude of both the solar and thermal path radiances is a direct result of the amount of atmospheric absorption and scattering, primarily from water vapor and aerosols, respectively. Both radiance components increase with increasing humidity and aerosol turbidity. The surface components (reflected infrared and solar and thermal emitted) are also affected, but in a different manner. The transmission of the surface emitted radiance is attenuated more for a murkier path, as is the downwelling radiance reflected by the surface back towards the sensor. For the MWIR window region (3.4 – 4.1 μm), the TOA radiance is dominated by the surface components, which make up from 80 - 95% of the total radiance depending on the atmospheric conditions. The remaining 5 – 20% is due to the path thermal emissions with a small amount from scattered solar radiation. Beyond the CO₂ absorption band, the contribution to the TOA radiance from surface-reflected solar or thermal radiation is very small even for very dry conditions (less than 2% at 5 μm).

4. MWIR TRANSFER

The transfer of radiation in the MWIR must include both solar reflected and thermal emitted components. Separate equations can be written for each radiance source. For clear-sky conditions, assuming a plane-parallel atmosphere and a Lambertian surface, the upwelling radiance at the sensor (or TOA) L_S^m due to scattered solar radiation can be expressed by⁸,

$$L_S^m = L_S^\uparrow + \frac{(1 - \epsilon_s)L_S^\downarrow}{1 - S(1 - \epsilon_s)} t \quad , \quad (1)$$

where L_S^\uparrow is the scattered path radiance at the sensor and L_S^\downarrow is the total (diffuse and direct) solar radiance that reaches the surface, ϵ_s is the surface emissivity, t is the atmospheric transmittance for the surface to sensor path and S is the spherical albedo. A dependence on wavelength is assumed for each parameter. The two terms on the right-hand side of (1) are the scattered path radiance and the surface reflected radiance. The “adjacency effect” term has not been included here, which is equivalent to assuming that the target and surrounding background emissivities are the same. The direct component of the downwelling solar radiance at the surface is given by the formula,

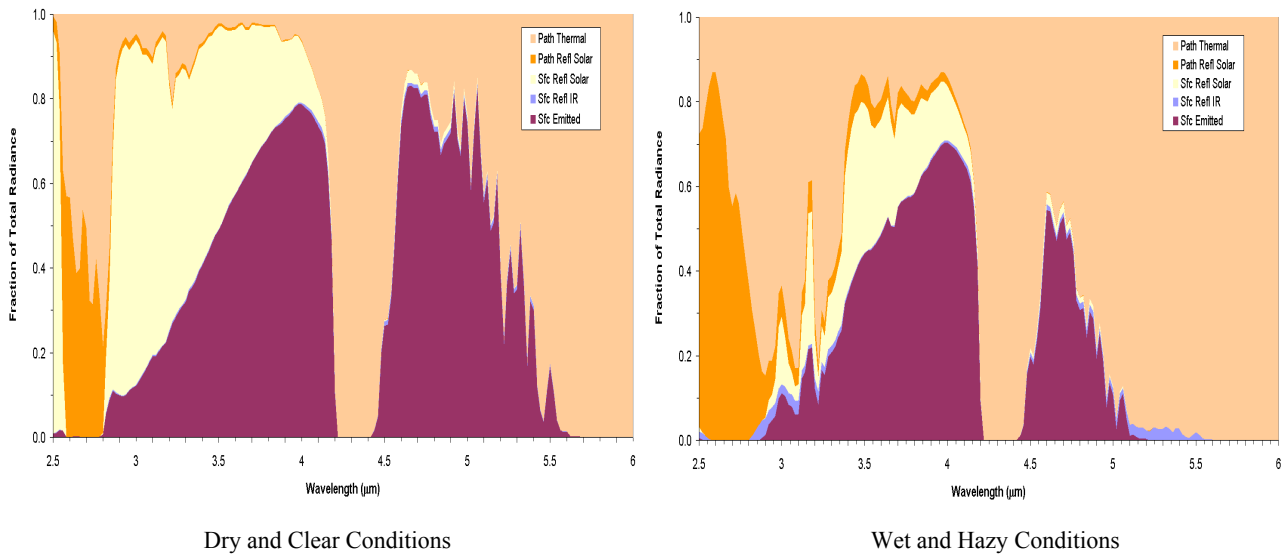


Figure 6. Plots of the five radiance components for the two sets of atmospheric conditions are shown. The plots depict the fraction of the total radiance for each component displayed in a stacked plot.

$$L_{S,dir}^{\downarrow} = \frac{F_0}{\mu_0 d_m^2} t_0 . \quad (2)$$

Here F_0 is the solar radiance at the TOA, μ_0 is the cosine of the solar zenith angle, d_m is the earth-sun distance ratio and t_0 is the transmission from the TOA to the surface along the sun to surface path. The diffuse component of the downwelling solar radiance is due to multiple scattering by atmospheric molecules and particulates and can be computed by multiple scattering codes such as DISORT n -stream⁹, which is packaged with Modtran.

For thermally emitted and absorbed radiation, using the same assumptions as before, the upwelling radiance at the sensor (or TOA) L_T^m under clear-sky conditions can be expressed by¹⁰,

$$L_T^m = \varepsilon_s B(T_s) t + L_T^{\uparrow} + \frac{(1 - \varepsilon_s) L_T^{\downarrow}}{1 - S(1 - \varepsilon_s)} t . \quad (3)$$

In (3), L_T^{\uparrow} is the thermal path radiance at the sensor and L_T^{\downarrow} is the downwelling thermal radiance at the surface, B is the Planck function, and T_s is the surface skin temperature. As before all parameters have a dependence on wavelength. The three terms on the right-hand side of (3) represent the surface emitted thermal radiation, the path radiance, and the reflected downwelling thermal radiance components of the total measured radiance at the sensor, respectively. Equations (1) and (3) can be combined to provide the total radiance received at the sensor (or TOA),

$$L^m = \left(L_T^{\uparrow} + L_S^{\uparrow} \right) + t \left\{ \varepsilon_s B(T_s) + (1 - \varepsilon_s) \left(\frac{L_T^{\downarrow} + L_S^{\downarrow}}{1 - S(1 - \varepsilon_s)} \right) \right\} . \quad (4)$$

The first term on the right is the total path radiance from both scattered solar and thermal emitted components. The second term is the radiance from the surface either from thermal emission or from reflection of downwelling solar or thermal radiation. The total at-sensor radiance for the MWIR can be divided into three components, the path radiance, the surface emitted, and surface reflected downwelling radiance.

5. ATMOSPHERIC COMPENSATION

In the VNIR/SWIR spectral region where reflected solar radiance is the primary source of radiant energy, the primary product of atmospheric compensation models is to recover the spectral surface reflectance. For spectral regions dominated by infrared radiative transfer, the primary product of atmospheric compensation models is still the surface reflectance (or more commonly the surface emissivity), however, the complex relationship between surface emissivity and temperature requires an extra step to the atmospheric compensation process. The first step retrieves the surface-leaving radiance by compensating for atmospheric effects in a manner similar to that used in the VNIR/SWIR. The surface-leaving radiance can be defined as $L_{sfc} = \varepsilon_s B(T_s)$. The second step requires the separation of the temperature and emissivity components of L_{sfc} using one of many techniques appropriate to the type of sensor making the measurements¹¹.

From Figure 6, it is apparent that some terms in (4) contribute more to the overall at-sensor radiance than others. The path-reflected solar radiance and the surface-reflected downwelling thermal radiance together provide between 1 and 4 percent of the radiance received at the sensor in the MWIR window. Below 3 μm , the path reflected solar radiance appears to provide a significant contribution, but due to the very small source radiance this contribution is essentially negligible. Neglecting these two terms for now, we can simplify (4) slightly,

$$L^m \cong L_T^{\uparrow} + t L_{sfc} + \frac{t(1 - \varepsilon_s) L_S^{\downarrow}}{1 - S(1 - \varepsilon_s)} , \quad (5)$$

For this spectral region, there are now three terms that combine to approximate the cloud-free at-sensor radiance: the path thermal (5-18%), the surface emitted (56-65%) and the reflected downwelling solar radiance (22-30%), with relative contributions to the MWIR window at-sensor radiance shown in parenthesis. Beyond the 4.25 μm CO₂ band, the solar component diminishes so the third term in (5) can be neglected,

$$L^m \cong L_T^\uparrow + t L_{sfc}, \quad \lambda > 4.5 \mu\text{m}. \quad (6)$$

Equations (5) and (6) contain two thermal radiance terms plus a solar reflectance term from which the surface leaving radiance can be obtained,

$$L_{sfc} = \frac{L^m - L_T^\uparrow}{t} - \left[\frac{(1 - \epsilon_s) L_S^\downarrow}{1 - S(1 - \epsilon_s)} \right], \quad (7)$$

where the second term on the right is needed for processing at wavelengths less than 4.5 μm . One problem with (7) is immediately apparent: both L_{sfc} and the reflected solar term are functions of ϵ_s . One method to circumvent this is to assume a constant value for the emissivity in the reflected solar term. For high emissivities ($\epsilon_s > 0.9$), and nominal values for the spherical albedo ($S \sim 0.1$), the solar reflected term can be approximated by $(1 - \epsilon_s) L_S^\downarrow$. Therefore, a typical emissivity variation in the MWIR window of 5-10% would result in an error in the magnitude of the reflected solar term of a similar amount (5-10%). Considering the magnitude of L_S^\downarrow which is typically small (0.04 – .16 W/m²-sr- μm), the effect of this assumption would be on the order of 0.01 W/m²-sr- μm . The estimated total radiance in the MWIR window ranges from 0.15 to 0.60 W/m²-sr- μm , so the error in making this assumption would be in the range of 2-5%. A further simplification to (7) with these assumptions would result in

$$L_{sfc}^* = \epsilon_s (B[T_s] - L_S^\downarrow) = \frac{L^m - L_T^\uparrow - t L_S^\downarrow}{t}. \quad (8)$$

The quantity L_{sfc}^* represents the total surface leaving radiance (a combination of the thermal emitted and reflected downwelling solar radiance). The unknowns in (8) are the upwelling thermal radiance at the sensor, the downwelling solar radiance at the surface, and the atmospheric transmission. Spectral values for these variables can be estimated from radiative transfer model calculations using scene appropriate model inputs to obtain an estimate of the total surface leaving radiance in the MWIR. Equation (8) can be expanded to include components that were previously neglected (downwelling thermal radiance and the reflected path solar radiance) to minimize errors incurred by their exclusion.

Techniques that might be used to solve (8) would all require a sufficient knowledge or estimate of the atmospheric conditions. Estimating the profiles of temperature and humidity is an important step to accurately determining the transmittance between the sensor and the surface using a radiative transfer model such as Modtran. With a goal of fast and efficient atmospheric compensation, a forward modeling approach using large multi-dimensional look-up-tables created from a series of Modtran runs could be used to provide estimates of the required parameters. These tables should include sensitivities due to atmospheric water vapor and aerosols (the primary variable atmospheric constituents). Specific conditions such as very dark pixels ($\epsilon_s \sim 1$) in the MWIR window could provide information on the thermal components of (8). While this is a valid and useful step in processing LWIR measurements, the spectral variability of the surface emissivity being greater in the MWIR than in the LWIR makes the application more difficult.

6. SUMMARY

The spectral and radiometric characteristics of the radiative transfer process in the MWIR have been examined. The effects of mixed gases are numerous in the MWIR, although much of the spectral region is dominated by water vapor and carbon dioxide absorption. Aerosols were found to still have an influence in the MWIR and should be included in any radiative transfer calculations. Surface emissivity varies less than in the VNIR/SWIR, with typical values at or above

0.85. Combining radiative transfer equations for both the solar reflective and the thermal emissive regimes, and neglecting terms that provided minimal contributions to the overall at-sensor radiance, the expected at-sensor radiance could be estimated. From this a simplified equation for the surface-leaving radiance including both solar and thermal components was derived. Limited availability of MWIR data precluded application of the technique at this time.

ACKNOWLEDGMENTS

The authors acknowledge support for this work by Mr. Ernie Reith and Mr. Wayne Hallada of the National Geospatial-Intelligence Agency. This work was sponsored by the Department of Defense under Contract F19628-00-C-0002. Opinions, interpretations, conclusions and recommendations are those of the authors and not necessarily endorsed by the United States Government.

REFERENCES

1. Griffin, M.K. and H.K. Burke, "Compensation of Hyperspectral Data for Atmospheric Effects," *Lincoln Laboratory Journal*, **14**, 29-54, 2003.
2. Malkmus, W., "Random Lorentz Band Model with Exponential-tailed S Line Intensity Distribution Function," *J. Opt. Soc. Am.*, **57**, 323-329, 1967.
3. Berk, A, L.S. Bernstein, G.P. Anderson, P.K. Acharya, D.C. Robertson, J.H. Chetwynd, and S.M. Adler-Golden, "MODTRAN Cloud and Multiple Scattering Upgrades with Application to AVIRIS," *Remote Sens. Environ.*, **65**, 367-375, 1998.
4. McCartney, E.J., *Optics of the Atmosphere; Scattering by Molecules and Particles*, John Wiley & Sons, New York, NY, 408 pp.
5. Shettle, E.P., and R.W. Fenn, "Models for the Aerosols of the Lower Atmosphere and the Effects of Humidity Variations on Their Optical Properties," *AFGL TR 79-0214*, Air Force Geophysics Laboratory, Hanscom AFB, MA, 94 pp, 1979.
6. Becker, F., "The Impact of Spectral Emissivity on the Measurement of Land Surface Temperature from a Satellite," *Int. J. Remote Sens.*, **11**, 369-394, 1987.
7. Griffin, M.K., S.M. Hsu, H.K. Burke, and J.W. Snow, "Characterization and Delineation of Plumes, Clouds and Fires in Hyperspectral Images," *SPIE* **4049**, 274-283, 2000.
8. Vermote, E.F., N. El Saleous, C.O. Justice, Y.J. Kaufman, J.L. Privette, L. Remer, J.C. Roger and D. Tanre, "Atmospheric Correction of Visible to Middle-Infrared EOS-MODIS Data Over Land Surfaces: Background, Operational Algorithm and Validation," *J. Geophys. Res.*, **102**, 17131-17141, 1997.
9. Stamnes, K., S.-C. Tsay, W. Wiscombe and K. Jayaweera, "Numerically Stable Algorithm For Discrete-Ordinate-Method Radiative Transfer In Multiple Scattering and Emitting Layered Media," *Appl. Opt.*, **27**, 2502-2509, 1988.
10. Gu, D., A.R. Gillespie, A.B. Kahle, and F.D. Palluconi, "Autonomous Atmospheric Compensation (AAC) of High Resolution Hyperspectral Thermal Infrared Remote-Sensing Imagery," *IEEE Trans.on Geos. & Rem. Sens.*, **38**, 2557-2570, 2000.
11. Caselles, V., E. Valor, C. Coll, and E. Rubio, "Thermal Band Selection for the PRISM Instrument 1. Analysis of Emissivity-Temperature Separation Algorithms," *J. Geophys. Res.*, **102**, 11145-11164, 1997.